

Article

Flexural Behavior of Precast RC Deck Panels with Cast-in-Place UHPFRC Connection

Zhe Zhang ¹, Yang Zhang ^{2,*} and Ping Zhu ²¹ School of Civil Engineering, Hunan University of Technology, Zhuzhou 412007, China² Key Laboratory for Wind and Bridge Engineering of Hunan Province, College of Civil Engineering, Hunan University, Changsha 410082, China

* Correspondence: zhangbridge@hnu.edu.cn

Abstract: Precast concrete bridge structures have been extensively used because of the mature construction techniques, fast construction, and their economy. Considerable practical applications, however, present certain disadvantages, such as cracking and water infiltration in their normal strength concrete (NSC, compressive strength 40 MPa) joints connecting prefabricated deck panels. Ultra-high performance fiber reinforced concrete (UHPFRC, compressive strength 143 MPa) has been proven highly effective in replacing the conventional cementitious grout materials in precast bridge structures. In the present study, three types of UHPFRC connections, rectangular, zigzag-shaped, and diamond-shaped, were experimentally evaluated on their flexural capacities, interface bonding performances, and failure modes through four-point bending tests (loading rate 0.1 kN/s). The results showed that all the UHPFRC connections exhibited apparently higher flexural capacities than an intact precast NSC member and had such strong UHPFRC-NSC interfacial bonding that the interfacial first-crack strengths were not less than the NSC member. Having the capability of modeling the UHPFRC connections and their interface properties, the developed finite element (FE) models of the precast slabs with UHPFRC connections produce numerical results in good agreement with the flexural tests. By means of the FE models, parametric investigations were carried out to make suggestions on optimizing the UHPFRC connection designs for practical use.

Keywords: ultra-high performance fiber reinforced concrete (UHPFRC); cast-in-place (CIP); normal strength concrete (NSC); UHPFRC connection; UHPFRC-NSC interface; flexural test; finite element analysis (FEA)



Citation: Zhang, Z.; Zhang, Y.; Zhu, P. Flexural Behavior of Precast RC Deck Panels with Cast-in-Place UHPFRC Connection. *Coatings* **2022**, *12*, 1183. <https://doi.org/10.3390/coatings12081183>

Academic Editor: Edoardo Proverbio

Received: 28 June 2022

Accepted: 8 August 2022

Published: 15 August 2022

Publisher's Note: MDPI stays neutral with regard to jurisdictional claims in published maps and institutional affiliations.



Copyright: © 2022 by the authors. Licensee MDPI, Basel, Switzerland. This article is an open access article distributed under the terms and conditions of the Creative Commons Attribution (CC BY) license (<https://creativecommons.org/licenses/by/4.0/>).

1. Introduction

The prefabricated concrete bridge elements and systems have been widely utilized owing to the mature construction technologies, fast construction, their economy, etc., [1]. However, in traditional prefabricated concrete bridges such as a decked T-girder concrete bridge, their precast superstructure elements are often interconnected longitudinally at their top flanges with cast-in-place (CIP) normal strength concrete (NSC) connections that usually become the vulnerable structural components, especially at their interface [2]. A lot of engineering applications show that the issues associated with cracking, water infiltration, and even severe damage at the CIP connections have been commonly found in many existing prefabricated T-shaped, pi-shaped, and box girder bridges, much to the detriment of the structural serviceability, durability, and safety. These issues mainly result from the low bonding strength of the new-to-old concrete interfaces at the CIP connections. Because the old concrete possesses a strong hydrophilic property, there would be a very thin water film at the interface while casting the NSC connections, and thus an interfacial transition zone (ITZ) could form with a relatively high water/cement (W/C) ratio between the new and old concrete. The interface transition zone that is usually rich in large crystals and is featured by highly porous structures normally causes a weak region and lowers the interface

bonding strength [3]. Furthermore, the coarse aggregates would tend to accumulate at the interfaces when the new concrete of the CIP connections is cast and vibrated, and they thus could be in point-to-point contact with the aggregate gravels or hardened cement paste protruding from the old concrete surfaces. Therefore, the fresh cement paste cannot easily flow through and fully saturate the interfacial transition zone, which would increase the number of voids in the ITZ and consequently weaken the interfacial bonding [4]. Moreover, the concrete shrinkage does not develop synchronously for the precast elements and CIP connections that are normally cast at remarkably different times of construction. Additional stresses associated with different shrinkage development between the new and old concrete might further lead to the weakening of the interfacial bonding performance [5].

Ultra-high performance fiber reinforced concrete (UHPFRC) is a type of fiber-reinforced cementitious composite characterized by high tensile and compressive strengths, durability, small aggregate size, a low W/C ratio (w/c), etc., [6–11]. Motivated by these superior properties, researchers have attempted to replace the conventional cementitious grout materials with UHPFRC in recent years. The low W/C ratio (normally 0.16–0.20) of UHPFRC relative to NSC (normally $w/c = 0.3–0.5$) could result in a thinner water film at the interface and the denser ITZ with lower porosity, which certainly improves the interfacial bonding between NSC and UHPFRC. Additionally, dissimilar to the conventional CIP NSC connections, the UHPFRC-NSC interface possesses no point-to-point contact due to no coarse aggregates contained in UHPFRC. Moreover, because of the self-compacting property, the fresh UHPFRC can easily fill the void or space on the rough old concrete surfaces when casting a UHPFRC connection. These would also benefit the formation of the interlock and development of the interfacial bonding strength of the field-cast UHPFRC connections [12].

Recently, investigators have conducted several experimental studies regarding the field-cast UHPFRC connections and the interfacial bonding performance between NSC and UHPFRC members. Tayeh and his colleagues performed the slant shear and splitting tensile tests of NC-UHPFRC composite specimens to evaluate the effects of the differently roughened surface textures of old concrete substrates on the mechanical bonding behaviors of interfaces [13,14]. They found that a sand-blasted surface provides the best interface bonding performance. Through the permeability tests, they also proved that the interfacial bonding is strong enough to put the NC-UHPFRC composite structures to good use. In similar investigations, Carbonell et al. [15,16] have also demonstrated that composite specimens having the UHPFRC-NSC interfaces with excellent long-term bonding performance carry high compressive, tensile, and shear stresses, regardless of the specimens' ages, the roughness degrees at old concrete surfaces, and whether or not experiencing exposure to freeze-thaw cycles. The above studies were mainly aimed at applications of a new UHPFRC overlay to the rehabilitation of concrete substrates. Owing to the good bonding performance of a UHPFRC-NSC interface, UHPFRC is considered for precast concrete bridge decks as a promising alternative to the conventional grout materials in shear keys or connections to avoid longitudinal cracks often observed therein. To evaluate the cracking resistance and enhancement of load transfer of UHPFRC connections, the direct shear, direct tension, and flexural tests [17] were carried out on the shear key specimens whose configuration was proposed by FHWA (Federal Highway Administration, US) [18]. The experimental results showed that the UHPFRC shear key presented a superior performance on the bearing capacity, interfacial bonding strength, and load transfer in comparison to all other conventional grout material types. For assessment of the behaviors of UHPFRC bridge deck connections, Graybeal carried out the flexural tests of full-depth precast deck panel specimens with CIP UHPFRC connections (diamond-shaped shear keys) under static and cyclic loading [19]. The results proved that the structural performance of the field-cast UHPFRC connections can meet or exceed that of the conventional CIP ones. Arafa et al. [20] attempted to investigate the applicability and performance of a UHPFRC joint connecting two precast GFRP (glass fiber-reinforced polymer) reinforced concrete elements and discussed the effects of the reinforcement types and axial stiffnesses. They concluded that the

reinforcement ratio and its modulus of elasticity have significant effects on the crack-width control and ultimate capacity. With past research endeavors and achievements, researchers have already put the concept of creating CIP UHPFRC connections between adjacent precast concrete girders into practice in several newly built concrete bridges [21]. These research results and successful applications demonstrate that the UHPFRC connections possess outstanding structural behaviors and their potential and promising applications will definitely facilitate the implementation and development of accelerated bridge construction, offer an effective solution to the rehabilitation of infrastructure, and mitigate the cracking risk of traditional precast concrete bridges at their connections.

2. Research Significance

The focus of the aforementioned research is mostly on the bonding performance and mechanical behaviors of rectangular and diamond-shaped UHPFRC connections using the splitting tensile, slant shear, or flexural tests. For the purposes of systematically and comprehensively comparing and assessing the structural bending performance and cracking resistance properties, three types of CIP UHPFRC connections, rectangular, zigzag-shaped, and diamond-shaped, were developed in the present study. Special attention was given to the effects of the interface treatments of the connections by using the flexural tests. Further, three-dimensional finite element (FE) models were created, which were capable of representing the NSC-UHPFRC interface behavior accurately, and were validated by the experimental results. The FE models were then used to numerically analyze the effects of interfacial performance between UHPFRC and NSC with different reinforcement ratios and surface treatments and to make suggestions on optimizing the UHPFRC connection designs for practical use.

3. Experimental Investigation

3.1. Material Properties

The UHPFRC used in the present study was developed by our research team, and its constituents and mix design are given in Table 1. The high-strength hooked-end steel fibers embedded in UHPFRC are 13 mm in length and 0.2 mm in diameter with a tensile strength over 2000 MPa. The polycarboxylic-based high-range superplasticizer adopted in the UHPFRC is able to reduce water demand even by 30%. According to the Chinese specification for mix proportion design of ordinary concrete [22], the normal strength concrete of Grade C40 was designed (see Table 1).

In accordance with the standards for the test methods of the mechanical properties of the NSC and UHPFRC [23,24], 150 mm and 100 mm cube specimens were prepared for measuring the compressive strengths of NSC and UHPFRC, respectively. The 150 mm by 150 mm prism specimens with lengths of 300 mm and 600 mm, respectively, were then used to measure the modulus of elasticity and flexural strength of NSC, whereas the prismatic samples of 100 × 100 × 300 mm and 100 × 100 × 400 mm were cast for the corresponding mechanical property tests on UHPFRC. All these specimens in the property tests have been subjected to the curing regimes identical to those in preparing the deck panel specimens with the UHPFRC connections in the flexural tests. Table 2 presents the measured mechanical properties of the UHPFRC and NSC used.

The reinforcing bars utilized longitudinally in the deck panel specimens are hot-rolled ribbed steel rebars, Grade HRB400, with a diameter of 12 mm, which possess the elastic modulus and yield strength of 200 GPa and 459 MPa, respectively [25]. For the transverse reinforcement in the test specimens, the hot-rolled smooth HPB300 steel rebar with a diameter of 10 mm, was used and its elastic modulus and yield strength are 210 GPa and 336 MPa, respectively [25].

Table 1. Mix proportions for UHPFRC and NSC.

Concrete Type	Ingredient	Amount, (kg/m ³)
UHPFRC	Portland Cement	771
	Silica fume	154
	Fly ash	77
	Quartz sand (Max. size: 0.9 mm)	848
	Quartz powder	154
	Superplasticizer (Polycarboxylate)	20.1
	Water	181
	Steel fiber (2% by Volume)	157
	W/P ratio ^a	0.18
NSC	Portland Cement	451
	Coarse aggregate (Max. size: 20 mm (0.79 in.))	1206
	Fine aggregate	568
	Superplasticizer (Naphthalene sulfonate)	4.5
	Water	185
	W/C ratio	0.41

Notes: ^a W/P ratio stands for water/paste ratio herein.

Table 2. Measured mechanical properties of UHPFRC and NSC.

Concrete Type	Compressive Strength (MPa)	Modulus of Elasticity (GPa)	Modulus of Rupture (MPa)
UHPFRC	143.2	42.0	21.4
NSC	40.2	32.8	6.2

3.2. Deck Panel Specimens

In the superstructures of numerous prefabricated concrete bridges, the top flanges of two adjacent modular components such as T-shaped and box girders, are frequently longitudinally joined with CIP connections that mainly carry transverse bending moments generated by live loads. The longitudinal CIP connection should have the same depth as the top flange, which is set to approximately 150 mm in many practical cases. Its transverse width needs to meet the minimum anchorage length requirement for the rebars into the connection. According to the loading transfer pattern in the CIP connections, five sets of deck panel specimens with UHPFRC joints were designed to assess their flexural and cracking behaviors by means of the four-point bending test in the present study. Among them, three types of UHPFRC connections, i.e., rectangular, zigzag-shaped, and diamond-shaped, were considered, and the corresponding deck panel specimens with these UHPFRC joints were designated as J-R, J-Z, and J-D, respectively. Based on the UHPFRC-NSC interface properties [26], the rough surface where coarse aggregates were exposed and which was recommended by Graybeal [18,19], was adopted for all specimens with the UHPFRC joints. In order to further enhance the interfacial bonding performance, we drilled three mortise holes from the interface into the precast NSC elements in one group of specimens of J-R that was then named J-R2. Furthermore, the reinforcement ratio within the UHPFRC connections definitely plays a major role in the flexural property of the investigated deck panels. Therefore, we specified a higher reinforcement ratio for the rectangular UHPFRC connection in specimens of J-R3. For comparison purposes, two control groups of monolithic deck panel specimens made of, respectively, NSC and UHPFRC were fabricated and labeled by M-N and M-U. After calculating the required anchorage length of the rebars in a UHPFRC connection according to the UHPFRC recommendations by AFGC, all the test

specimens were designed to have the same geometry of 1500 × 300 × 150 mm and their detailed information is provided in Table 3.

Table 3. Details of test specimens.

Specimen Type	Specimen Label	Material	Interface Treatment	Reinforcement Ratio (%) ^a	Joint Configuration
With Connections	J-R1	NSC/UHPFRC	Rough	4.02	Rectangular
	J-R2		Rough/hole	4.02	Rectangular
	J-R3		Rough	5.53	Rectangular
	J-Z		Rough	4.02	Zigzag-shaped
	J-D		Rough	4.02	Diamond-shaped
Monolithic	M-N	NSC	N/A	2.01	N/A
	M-U	UHPFRC	N/A	2.01	N/A

Notes: ^a The reinforcement ratio is within the UHPFRC connections that is different from that in the precast NSC elements due to non-contact lap-spliced rebars.

Figure 1 shows the geometric and reinforcement details of the test specimens, all of which were reinforced with two orthogonal grids of reinforcing bars vertically spaced at 110 mm (see Figure 1a). The longitudinal and transverse steel bars were respectively the rebars of N1 and N2, which were equally spaced at 80 mm and 100 mm. Each test specimen with a UHPFRC joint consisted of two identical precast NSC elements of 680 mm in length and a CIP UHPFRC component being 140 mm wide in-between. The longitudinal rebars of N1 in the two NSC blocks, protruded from the interfaces by a length of 130 mm and overlapped to form a non-contact lap splice of 120 mm in each UHPFRC connection. The configurations of the three types of UHPFRC joints and their interface treatments are illustrated in Figure 1b. The test specimens of J-R with the rectangular UHPFRC connection were divided into three groups to ascertain the contributions of the reinforcement ratio and mortise holes to the interfacial bonding performance. For each specimen of J-R2, the three mortise holes drilled were 25 mm in diameter by 50 mm in depth, whereas in the J-R3 specimens, the extra steel bars of Grade HRB400 with a diameter of 12 mm and a spacing of 80 mm were longitudinally added into the UHPFRC connections to increase the local reinforcement ratio by 1.5%. Contrary to the rectangular UHPFRC connection in a specimen of J-R, two trapezoid-shaped slots with a depth of 50 mm were vertically made at one end of a precast NSC element and then the zigzag-shaped joint configuration could be formed for the specimens of J-Z. The spacings of some longitudinal and transverse rebars in specimens J-Z thus needed to be adjusted locally for easy casting. In specimen J-D, two adjacent precast NSC elements with inward triangle-shaped transverse slots were joined by a diamond-shaped UHPFRC connection (See Figure 1b).

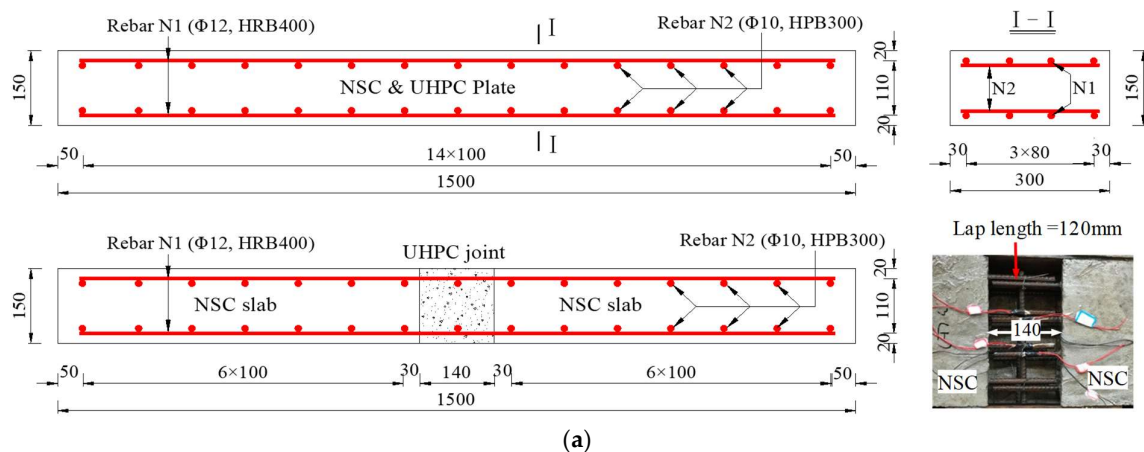


Figure 1. Cont.

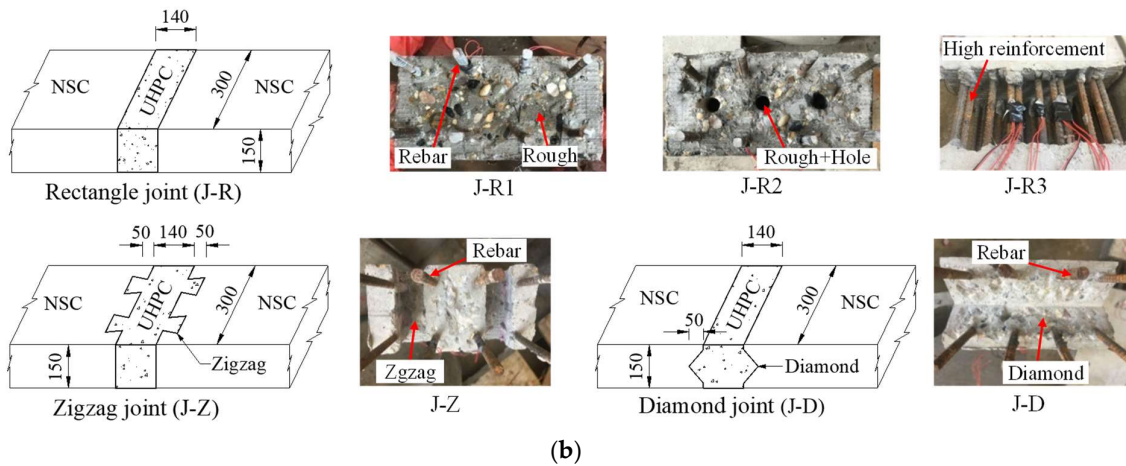


Figure 1. Test specimens: (a) Dimensions and reinforcement details; (b) UHPFRC joint types.

3.3. Fabrication of Specimens

The fabrication procedure illustrated in Figure 2 includes three stages for all test specimens. The specimens (M-N) made of NSC and the precast NSC components of the specimens with UHPFRC connections were first cast, which were then cured under a standard curing regime in a normal laboratory environment at an average ambient temperature of 26 °C for 60 days. After the curing procedure, a surface treatment at one end of each precast NSC component was carried out by roughening, drilling holes, and the combination of both, respectively. The surfaces with highly exposed aggregates needed to be prepared and then to be brushed to remove the loose particles with wire-brushes. For a similar purpose, the drilled mortise holes were also required to be cleaned of the debris. Since the saturated concrete surface can help to create a high cohesion between NSC and UHPFRC and thus to improve their bond performance [16], we kept water-saturating the ends of the precast NSC components until these surfaces have been fully saturated before pouring the UHPFRC connections. In the last stage, the monolithic deck panel specimens of M-U and the UHPFRC joints were cast and have been cured under an approximately constant temperature of 28 °C for 28 days prior to testing.

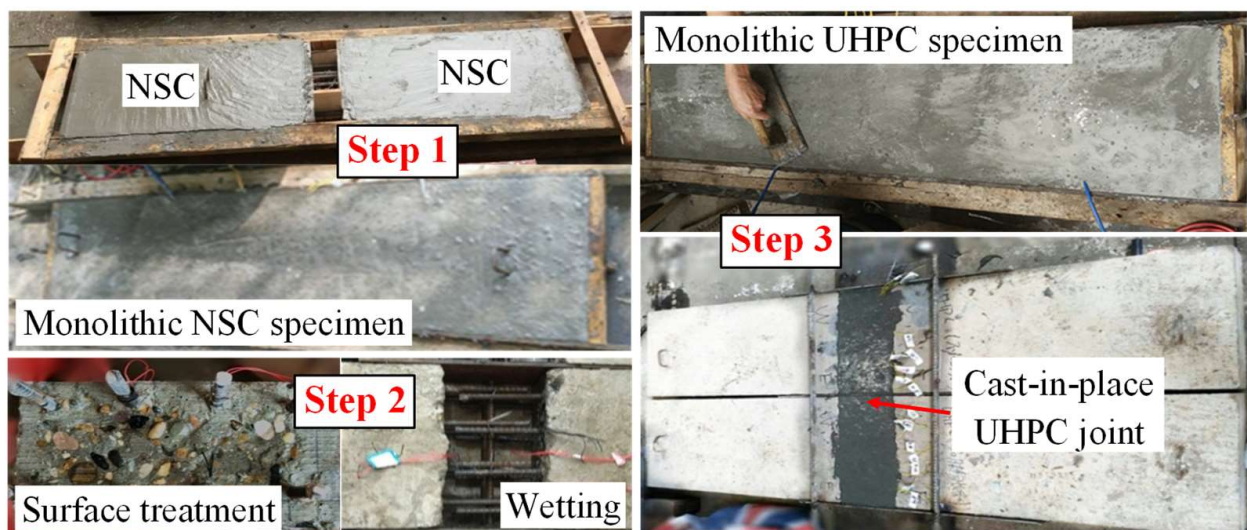


Figure 2. Fabrication of test specimens.

3.4. Test Setup, Apparatus, and Procedure

Figure 3 shows the test setup and the arrangement of measuring points for strain and deflection measurements in the four-point flexural tests. All the test specimens were simply

supported with a simple span of 1300 mm, and the two loading points symmetrically and centrally that were located about the midspan were spaced at 400 mm. A hydraulic jack was installed to apply the vertical loading at the midspan, which was measured with a load cell attached below and was equally divided and transferred through a steel spreader beam to the specimen. Strain gauges were mounted on the top and bottom surfaces of the test specimens as well as on the surfaces of reinforcing bars at the midspan. The vertical deflection of each test specimen was measured by the dial gages installed on the top of the specimen at the two end supports and on the bottom at the midspan and the two loading points.

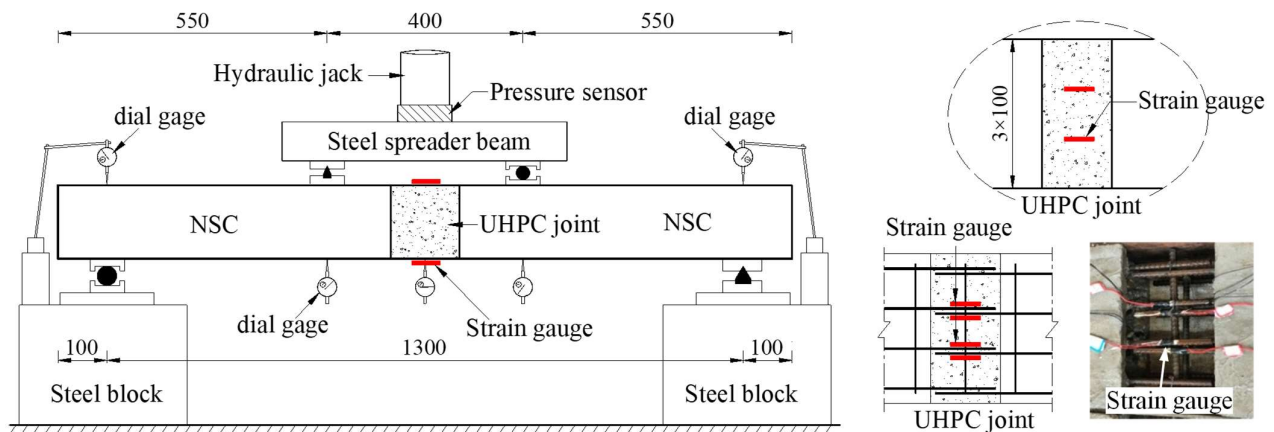


Figure 3. Test setup and arrangement of measuring points.

Prior to each flexural test, preloading was initially applied to the test specimens through four load steps until 12 kN to validate the loading system and instrumentation functioning normally. In the subsequent four-point bending tests, the specimens were loaded at a constant loading rate of 0.1 kN/s in multiple load steps until their failure. Each loading increment was set to be 4 kN per step. When each load level was reached, the loading was sustained for at least 5 min to record the measurements.

4. Experimental Results and Discussion

4.1. Load-Deflection Responses

In order to characterize the flexural behaviors of the bridge decks with connections and to facilitate comparisons among different connection types, the load versus midspan deflection curves were illustrated for the seven groups of specimens in Figure 4. Each curve was obtained by averaging the measurements of the specimens in one group. As shown in Figure 4, the flexural curves of the specimens with the UHPFRC joints are almost enveloped by the upper and lower solid test curves labeled by M-U and M-N.

Illustrated in Figure 4, the flexural behaviors can roughly be divided into three stages (represented by circled numbers 1–3) that are mainly determined by the linear elastic behavior, crack initiation and propagation, and reinforcing bar yielding, respectively. The load-deflection curve of the specimen of M-U, for example, does not exhibit a distinct fictitious transition point between the first two stages, since the change in the slope of the curve is not much differentiable. The second stage of this curve also reveals that the cracks initiated do not develop rapidly with the rising load, which accounts for a crack pattern, say, short, narrow, and densely distributed cracks, in a specimen of M-U. Once the embedded reinforcing bars yield, the midspan deflection of M-U would increase significantly, but the post-yielding stiffness of M-U still apparently exceeds all the other types of specimens.

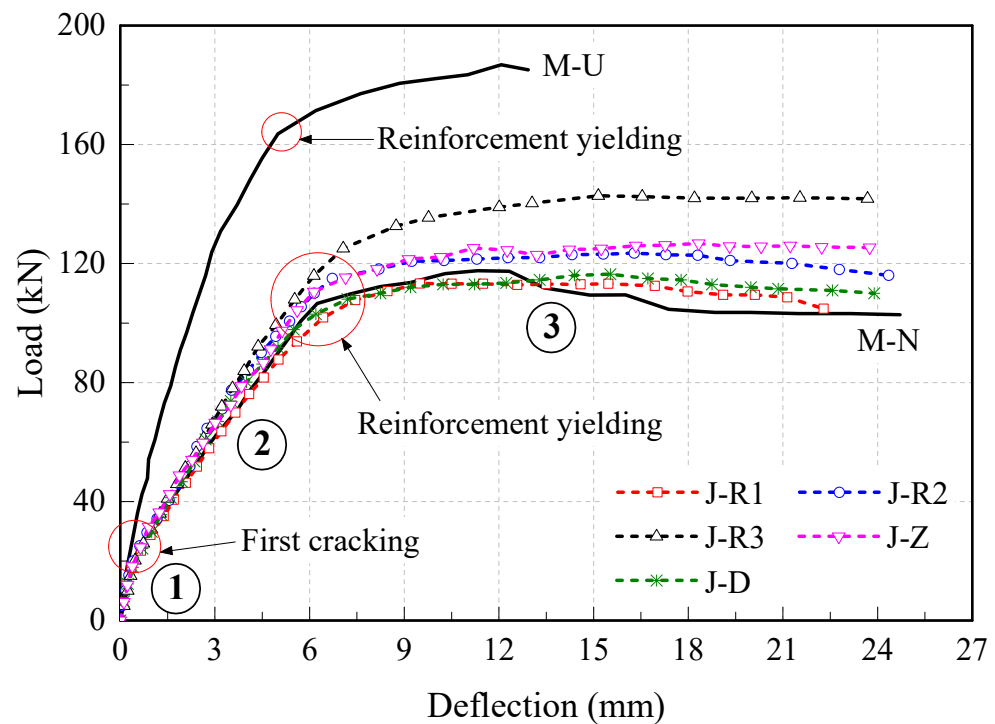


Figure 4. Load versus midspan deflection of the test specimens.

The specimens of the monolithic deck made of NSC and with UHPFRC connections exhibit a very similar flexural behavior in the stages of pre-yielding of the reinforcements. In the first stage, all the load-midspan deflection curves of these specimens almost coincide with each other, which means the application of a UHPFRC connection to connecting the prefabricated NSC deck panels could assure a comparable linear elastic behavior relative to a monolithic deck panel of NSC. According to Figure 4, the onsets of their first cracks in the specimens, defining the fictitious points of transition from the first stage, seem not to be distinguishable, but actually the corresponding first-crack loads for J-R2 and J-R3 are improved by up to 9% compared to M-N. It demonstrates that the first-crack strengths of bridge decks with UHPFRC connections are much influenced by the interfacial treatments, such as drilling mortise holes and adopting a higher reinforcement ratio within the connections. When entering the second stage, those curves, for specimens of J-R2, J-R3, and J-Z, start to deviate slightly upwards from that for the specimen of M-N, which indicates that cracks occur at different locations and develop up to different damage degrees in these specimens. The reinforcing bars might get involved to resist the entire tension on the tensile side earlier in the cracked specimen with more serious damage, and they also reach their yield points faster. Therefore, the specimens of J-R2, J-R3, and J-Z can carry relatively higher loads at their fictitious points of transition to the third stage than the others. In the last stage of the curves, except for M-U, the specimens could no longer support the load increment, and the dramatically increasing midspan deflections of the test specimens cause their final failure. Because of the locked mortises and tenons in J-R2, strengthening provided by the denser reinforcement in J-R3, and interlocking action of the zigzag-shaped UHPFRC-NSC interface in J-Z, however, these test specimens also still had a little larger remaining bending stiffness than M-N and other specimens with UHPFRC joints. In conclusion, all the specimens with UHPFRC connections under investigation exhibit the flexural performance, at least not less than the monolithic deck panel specimens made of NSC.

4.2. Load-Crack Width Relationship

As shown in Figure 5, we illustrated the load versus widths of main cracks as well as the cracks at UHPFRC-NSC interfaces for the test specimens. The relationship between the

load and main crack width plotted on the right side in the figure can be characterized by a bilinear model with a transition point that corresponds to the yielding of the reinforcement embedded in the specimens. In the phase of the pre-yield of the reinforcing bars, the widths of the main cracks almost increased equally with rising loads for specimens of M-N, J-R2, and J-R3, but slightly faster than those for the specimens of J-R1, J-Z, and J-D. After yielding of the reinforcements, the main crack widths have developed significantly for all groups of specimens, including M-U. These specimens also had nearly the same slope of the curves of the load—width of the main crack, except for J-R3, which might result from the higher reinforcement ratio used in the UHPFRC connection of J-R3. Generally, the monolithic specimens of NSC and those with UHPFRC connections presented comparable capabilities of resisting the main cracks since these main cracks initiated and propagated in the NSC components within the pure bending zones or at an interface.

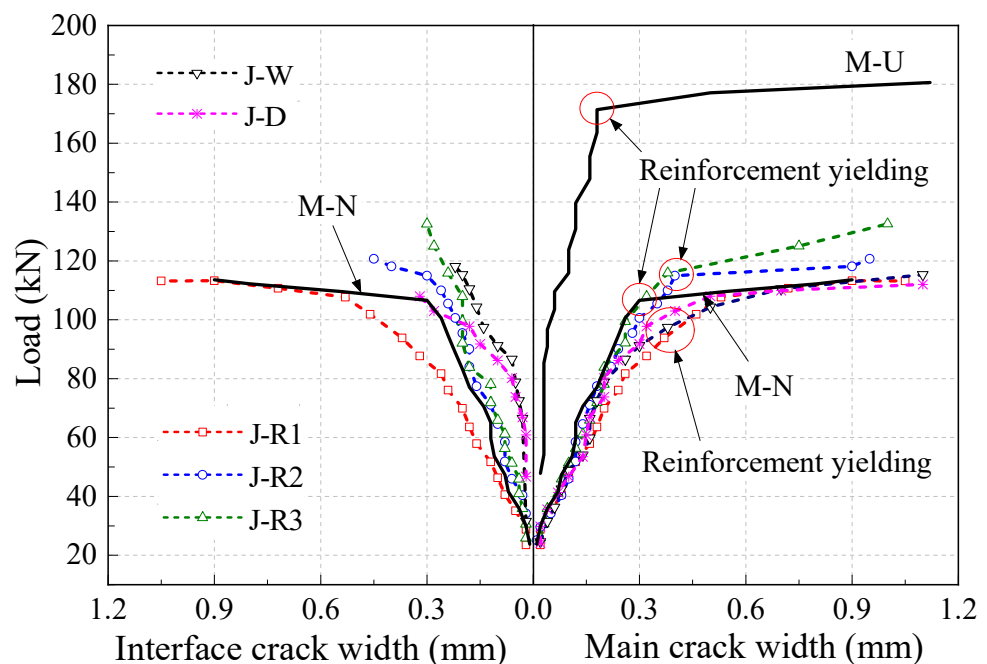


Figure 5. Load versus width of main crack and cracks at interface.

The curves on the left side of Figure 5, show the comparisons of the crack opening rates at their interfaces of test specimens. Among them, the curve for J-R1 is just mirror images of that on the right side, since the crack initiated at the interface of J-R1 has developed into the main crack. The width of this interfacial crack grew apparently faster than the monolithic specimen M-N, which meant the interface bonding could not render sufficient crack resistance just by this rectangular UHPFRC connection type without a certain interface treatment or a higher reinforcement ratio. For all the other types of specimens with UHPFRC connections, their interfacial crack opening rates almost varied linearly with loads, but these cracks did not turn into the main cracks. Compared with J-R1, the curves for J-R2 and J-R3 are very close to that for M-N, which also demonstrates that drilling mortise holes at the interface or raising the reinforcement ratios is an effective solution to achieve better bonding strength for the interface between NSC and UHPFRC. Moreover, the UHPFRC connection type, such as in J-Z and J-D, also highly affected the interfacial bonding performance, since we observed that their interfacial crack opening increased much slower than the others.

As specified in the Chinese code for the design of reinforced concrete and prestressed concrete bridges [27], the allowable maximum crack width is 0.2 mm for a reinforced concrete element. We thus recorded the loads, $MCW_{0.2}$ and $ICW_{0.2}$ that, respectively, corresponded to the widths of 0.2 mm for the main and interfacial cracks for all test specimens, and illustrated them in Figure 6.

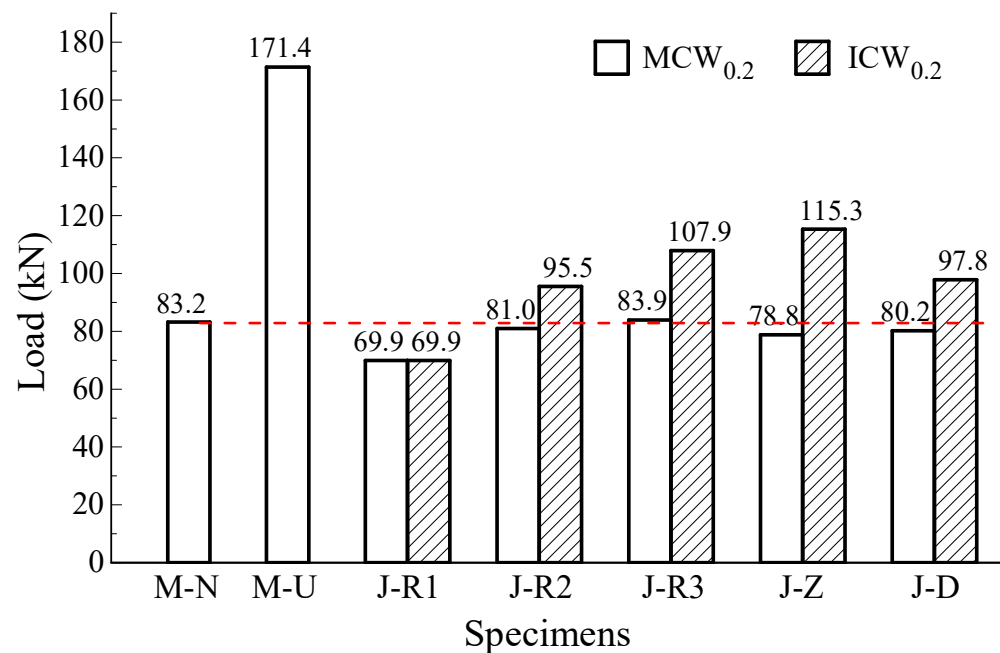


Figure 6. Loads corresponding to crack width of 0.2 mm.

As shown in this figure, the load that caused the main crack width of 0.2 mm in the monolithic deck panel specimen of UHPFRC is much higher than other specimens owing to the superior tensile and ductile properties of UHPFRC. The previous discussions are qualitatively based on the crack-resistance and interface bonding performance by the crack opening rates, and here we can quantitatively compare their flexural properties according to the loads, $MCW_{0.2}$. The formation of the main crack with a width of 0.2 mm at the interface of J-R1 led to a much lower load that decreased by 16% compared to the monolithic specimen M-N. The UHPFRC connection scheme used in J-R1 is thus the least applicable to prefabricated bridges as joints. Although the loads $MCW_{0.2}$ for J-D and J-Z were also slightly lower than the specimen M-N, it is convinced that in case of applying the interface treatment or the denser reinforcement as what we have done in J-R2 and J-R3, it would benefit the crack resistance for J-D and J-Z, in view of the greater loads $MCW_{0.2}$ for specimens J-R2 and J-R3 over J-R1. The comparisons of the loads, $ICW_{0.2}$, show that except for J-R1, the four groups of specimens with UHPFRC connections had sufficient interface bonding to resist loads, since loads of $ICW_{0.2}$ were increased by a range between 14.8% and 38.6% relative to $MCW_{0.2}$ for M-N. It is also confirmed that a combination of a UHPFRC connection type as in J-D and J-Z, and a feasible interfacial treatment and reasonable reinforcement ratio could construct a potential precast RC bridge deck with UHPFRC joint that has effective interfacial debonding resistance and flexural performance at least not less than a monolithic bridge deck panel made of NSC.

4.3. Crack Patterns and Failure Modes

Since the crack distribution and the failure mode for the specimens in each group were similar in the bending tests, we chose and illustrated the typical cracking patterns for the seven groups of test specimens in Figure 7. The loads of first cracks occurred in NSC components, within UHPFRC joints and at the interfaces, failure loads and locations of first and main cracks for the test specimens were tabulated in Table 4.

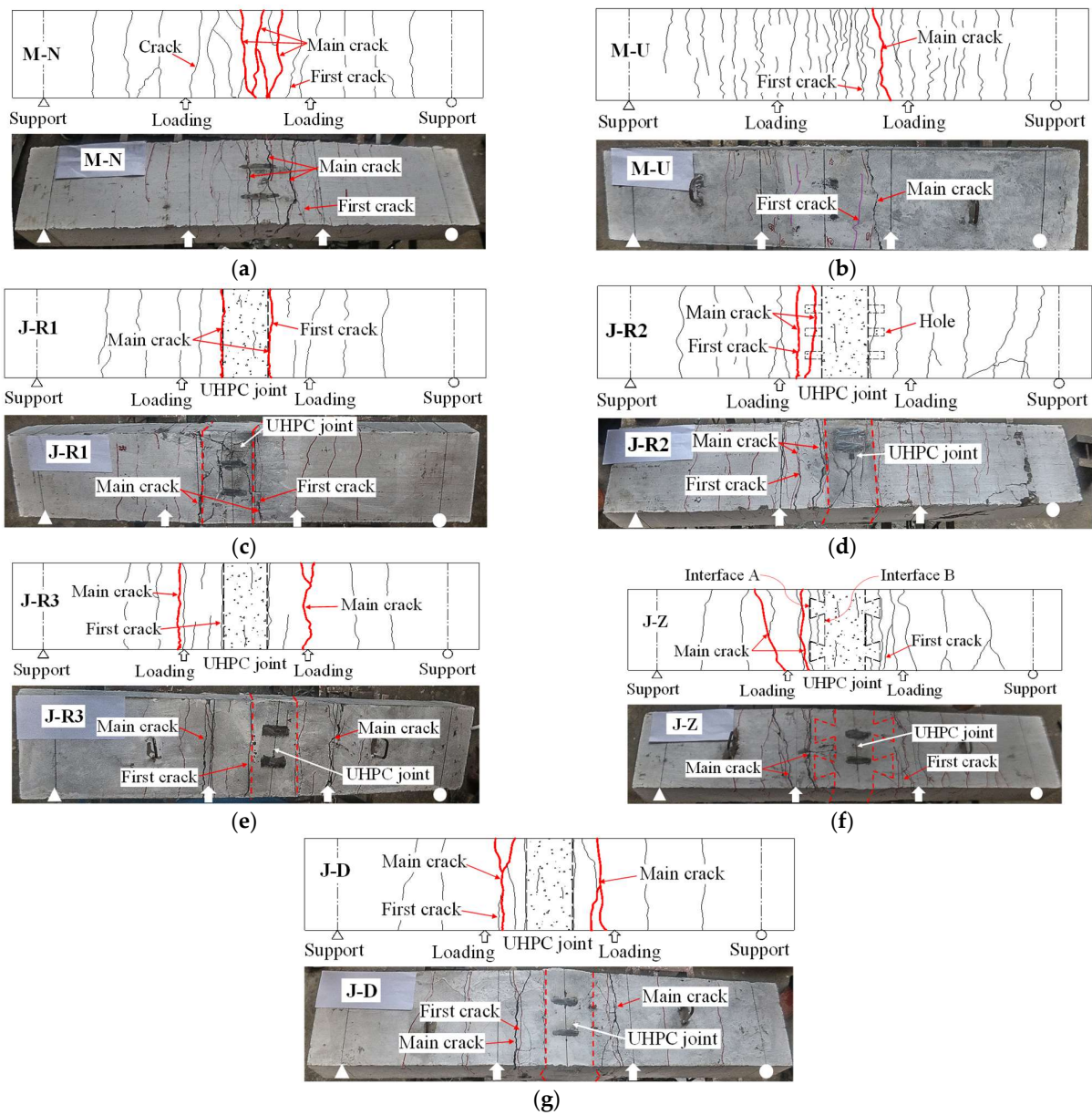


Figure 7. Cracking patterns and failure modes: (a) M-N; (b) M-U; (c) J-R1; (d) J-R2; (e) J-R3; (f) J-Z; (g) J-D.

Table 4. Crack details and corresponding loads (kN) of the specimens.

Specimens	First Crack Load (kN)	Location of First Crack	Load of First Crack at Interface (kN)	Failure Load (kN)	Location of Main Crack	Load of First Crack within Joint (kN)
M-N	23.8	NSC	N/A	117.6	NSC	N/A
M-U	47.8	UHPFRC	N/A	186.8	UHPFRC	N/A
J-R1	23.5	Interface	23.5	113.3	Interface	69.9
J-R2	25.1	NSC	34.2	123.5	NSC	77.4
J-R3	25.9	Interface	25.9	142.8	NSC	92.1
J-Z	24.6	NSC	31.5 (A)/59.8 (B) ^a	126.8	NSC	66.5
J-D	24.2	NSC	46.7	116.4	NSC	60.9

Notes: (1) ^a A and B herein represent the interfaces of A and B between NSC and UHPFRC for the specimens of J-Z.

For the monolithic deck panel specimens of M-N and M-U, their first transverse cracks appeared within the pure bending zone of specimens when the loadings, respectively, reached 23.8 kN and 47.8 kN (approximately 20% and 26% of their peak loads). Shown in Figure 7a,b, the cracks in the specimens of M-N tended to branch off and propagate radially. These specimens also had much fewer cracks than the specimens of M-U and possessed several main cracks at their failure. On the contrary, more cracks that were narrower and distributed more densely were observed in the specimens of M-U and only one main crack finally existed when the specimens failed.

Those specimens with UHPFRC connections, however, exhibited different characteristics in crack initiation and development that were much influenced by the connection type, interface treatment, and reinforcement ratio within the connections. In general, the cracks might most likely appear in the precast concrete components or at the UHPFRC-NSC interface because the UHPFRC connections were more crack resistant than NSC. There were thus only a few short and narrow cracks observed within the UHPFRC connections. We described specifically the crack patterns and failure modes for the three types of specimens with UHPFRC joints investigated in this study. The two kinds of specimens, J-R1 and J-R3, both had the first cracks at their NSC-UHPFRC interfaces at the loadings of, respectively, 23.5 kN and 25.9 kN (approximately 21% and 18% of their peak loads). Generally, these loadings were close to the first cracking load of the monolithic deck panel specimen M-N. Illustrated in Figure 7c,e, the main cracks in specimens J-R1 almost existed around the interface and their development resulted in the interfacial failure between NSC and UHPFRC and then the final failure of the specimens. However, for the specimens J-R3, the presence of a higher reinforcement ratio within the UHPFRC joint might suppress the development or propagation of the cracks initiating around the interface. The main cracks were thus formed in the precast NSC components instead of within the UHPFRC joints and led to the final failure of specimens J-R3. As presented in Figure 7d, the average load of 25.1 kN (about 20% of the failure load) gave rise to the crack initiation in the region between a loading point and the bottom of the mortise holes for specimens of J-R2. When the average loading increased to 34.2 kN (about 28% of the failure load), the cracks were observed at the UHPFRC-NSC interface, but the main cracks existed in the precast NSC components that would induce the failure of the specimens. An interesting observation was that shear cracks occurred in the shear span, which inclined approximately at an angle of 45°. For specimens of J-Z, two interfaces between NSC and UHPFRC were respectively labeled by A and B because of the configuration of the zigzag-shaped UHPFRC joint shown in Figure 7f. The crack first appeared 75 mm away from interface B in the precast NSC element at the load of 24.6 kN (approximately 19% of the peak load). Then, when the load reached 31.5 kN and 59.8 kN (approximately 25% and 47%), the first cracks were successively produced at the interfaces A and B. However, the crack opening rate has been flat with the further rising load and finally the failure of specimens J-Z was induced by the main cracks formed in the precast NSC elements. For specimens of J-D (see Figure 7g), the loads that caused the first cracks in the precast NSC elements and at the interface were 24.2 kN (about 21% of the failure load) and 46.7 kN (about 40% of the failure load), respectively. Similarly, this group of specimens possessed a parallel failure mode with specimens of J-Z. To sum up, except for specimens of J-R1 that had similar first-crack and flexural strengths to the monolithic specimens M-N, the other four types of deck panels with UHPFRC connections proved to be effective candidates for bridge deck applications, since they presented superior crack resistance and behaved better over the control specimens of M-N.

From Table 4, we can find that the UHPFRC connection had a significantly higher first-crack load than the load corresponding to the first crack that appeared in the rest of the specimen, and even than the first-crack strength of a monolithic deck specimen made of UHPFRC. Additionally, those cracks initiating within the UHPFRC connections propagated and developed slowly with the increasing loads. The weakness of a UHPFRC joint thus normally existed at its interface. For an entire specimen, however, the use of a UHPFRC connection would not necessarily lead to the weakening of its mechanical performance,

according to Table 4. The first cracks occurred at the interfaces in two among five groups of specimens with UHPFRC connections, J-R1 and J-R3, and the corresponding loads were very close to the first-crack strength of M-N. Therefore, we need to consider appropriate UHPFRC joint types, interfacial treatments, and reinforcement ratio to assure enough crack-resistance of bridge decks with UHPFRC connections for their engineering applications. In all groups of specimens, J-R1 had the weakest interfaces where the main crack formed to cause the final failure at a slightly lower load than the flexural strength of monolithic panel specimens of M-N. On the fracture surface of the UHPFRC joint in J-R1, much NSC as well as some aggregates were attached, which might result from the destabilization of the coarse aggregates in the surface roughening process. Although the first cracks were also initiated at the interfaces in the specimen J-R3, they grew slowly with rising loads and did not finally develop into the main cracks that were located in the precast NSC elements. For the other specimens with UHPFRC connections, J-R2, J-Z, and J-D, their first cracks occurred in the precast NSC elements and their loads of first crack at the interface exceeded the first crack strength of M-N by 43.7%, 32.4%, and 96.2%, respectively. The main possible reasons that these three types of NSC-UHPFRC interfaces performed better have been given as follows.

The UHPFRC filling the mortise holes drilled at the interface could enhance the interfacial crack resistance in J-R2.

The relatively larger interface areas in specimens J-Z and J-D could normally result in better bonding performance at interfaces. On the other hand, due to the presence of the non-planar interfaces, those interfacial micro-cracks could not grow and develop unrestrainedly along the interfaces.

With the propagation of the first cracks initiated in the precast NSC components in these three types of specimens, the reinforcing bars are involved to carry more loading at those cracked sections and in return the internal forces at their interfaces would increase relatively slowly. Why the loads of first cracks occurred within UHPFRC joints are much greater than the first crack strength of the monolithic panel specimens M-U could also be explained in a similar way.

According to the failure loads given in Table 4, the specimens of M-U definitely presented the highest failure load because of the superior properties of UHPFRC. Owing to the relatively denser reinforcement within the UHPFRC joints, the specimens of J-R3 also apparently exhibited a higher failure load than the rest of the specimens. In spite of less load-carrying capacities, the specimens of J-R2, J-Z, and J-D still possess comparative failure loads relative to M-N.

5. Finite Element Analysis

5.1. Finite Element Models

The numerical analysis of the flexural behaviors of the bridge deck panels with UHPFRC connection was conducted by using the commercially available finite element package, ABAQUS, in the present study. For comparison and validation purposes, we constructed seven finite element models and designated their respective labels corresponding to the seven groups of test specimens, and the FE model of J-D is shown in Figure 8 as an example. The FE models have the same dimensions as the corresponding deck panels with UHPFRC connection specified in Figure 1. In these FE models, two element types, C3D8R (8-node linear reduced-integration brick element) and T3D2 (three-dimensional 2-node truss element) were adopted for the UHPFRC and NSC components and the embedded reinforcing bars, respectively. The use of elements of C3D8R is capable of achieving efficient computations without losing accuracy, especially for the displacement solution. The embedded element technique was applied in defining the steel reinforcement with T3D2 elements. To accomplish a better compromise between the computational efficiency and accuracy, we refined the mesh locally within the regions such as the interface and UHPFRC joints based on the assigned global seeding size of 2 cm in the FE models. The loading and boundary conditions (simply supported) that have been applied to the FE models

were kept as much alike as possible to those of the test specimens in the previous flexural experiments (see Figure 3).

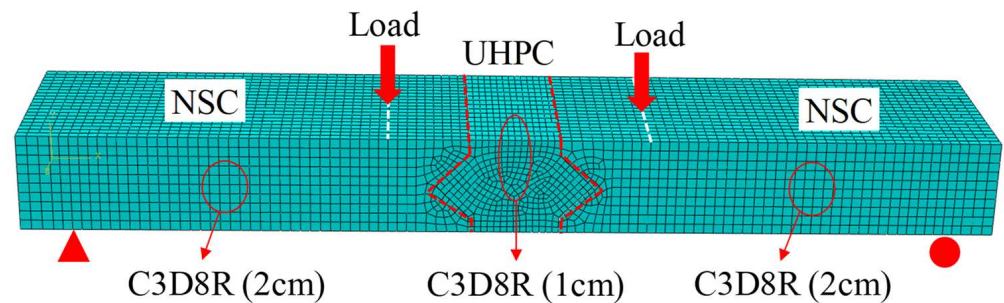


Figure 8. An example of finite element models (J-D).

The FE package ABAQUS offers two built-in inelastic constitutive models for concrete, namely the smeared crack and damaged plasticity models. The latter model is able to represent the inelastic behavior of concrete by combining scalar damaged elasticity and isotropic tensile and compressive plasticity [28], in which a scalar degradation variable is included to characterize the reduction of the elastic modulus of concrete. According to the research by Chen and Graybeal [28], the damaged plasticity model was used in the present FE analysis since the concrete smeared crack model might give rise to a convergence problem and exhibit a stiffer response in the nonlinear phase. The material parameters required for the damaged plasticity model of NSC and UHPFRC are listed in Table 5. Figure 9 shows the uniaxial tensile and compressive stress-strain relationships of UHPFRC and NSC adopted in this study. The steel reinforcing bars were considered as an elastic-perfectly plastic material for both in tension and compression.

Table 5. Material properties of NSC and UHPFRC adopted in FE models.

Material Property	UHPFRC	NSC
Mass density (kg/m^3)	2495 ^a	2408 ^a
Young's modulus (GPa)	42.0 ^a	32.8 ^a
Poisson's ratio	0.19 [28,29]	0.20 [30]
Dilation angle	15° [28,29]	30° [30]
Eccentricity	0.1 [28,29]	0.1 [30]
f_{b0}/f_{c0} ^b	1.16 [28,29]	1.16 [30]
K_c ^c	23 [28,29]	23 [30]
Viscosity parameter	0.0 [28,29]	0.001 [30]

Notes: (1) ^a The superscript a means that the labeled value is obtained from material tests. (2) ^b f_{b0}/f_{c0} is the ratio between the biaxial compressive strength and the uniaxial compressive strength. (3) ^c K_c is the ratio between the second stress invariant on the tensile meridian and that on the compressive meridian.

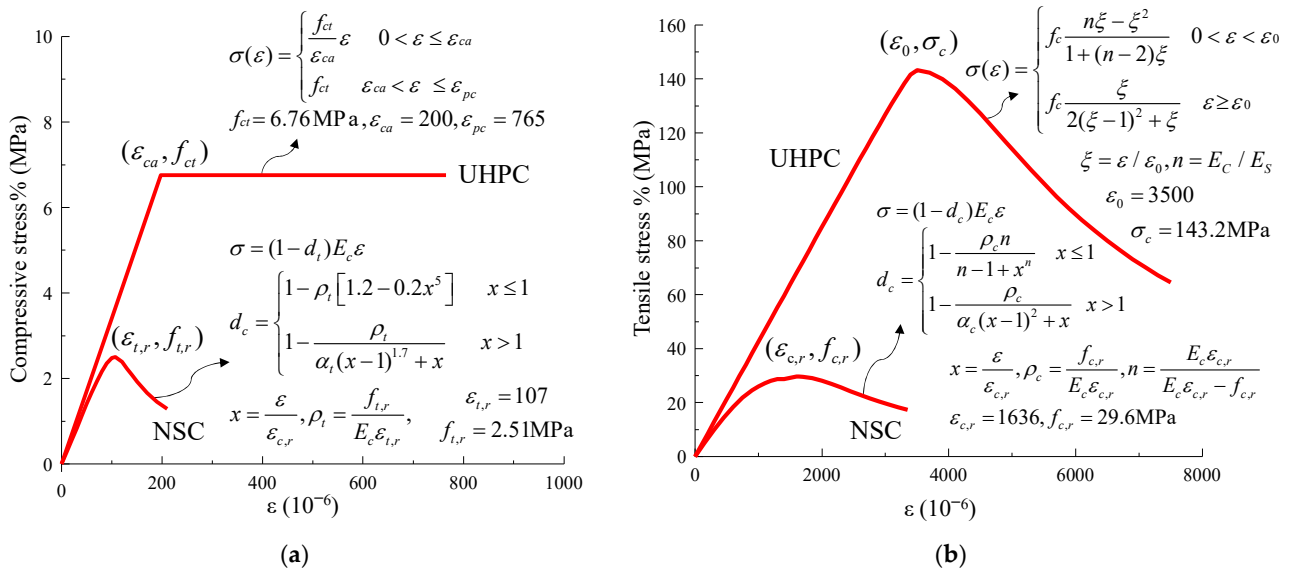


Figure 9. Uniaxial stress-strain relationships of UHPFRC and NSC: (a) Tension [25,31]; (b) compression [25,32].

5.2. Interface Modeling

For accurately simulating the flexural behavior of a deck panel with a UHPFRC connection, modeling the NSC to UHPFRC interface is crucial in FE models. Recommended by Hussein [33], a traction-separation constitutive relationship that takes into account the friction and adhesion at the interface was employed to capture the interface behavior. Shown in Figure 10, the adopted traction-separation model features two linear stages, an initially linear elastic response followed by a linear degradation caused by the damage initiation and evolution [34]. The parameters required to define the traction-separation model include the stiffness (K) relating to separation across the interface prior to damage initiation, the peak value of traction stress (t) at the interface, and the total plastic displacement (δ) at the failure of the interface. The parameter values used in the present study are given as follows [33].

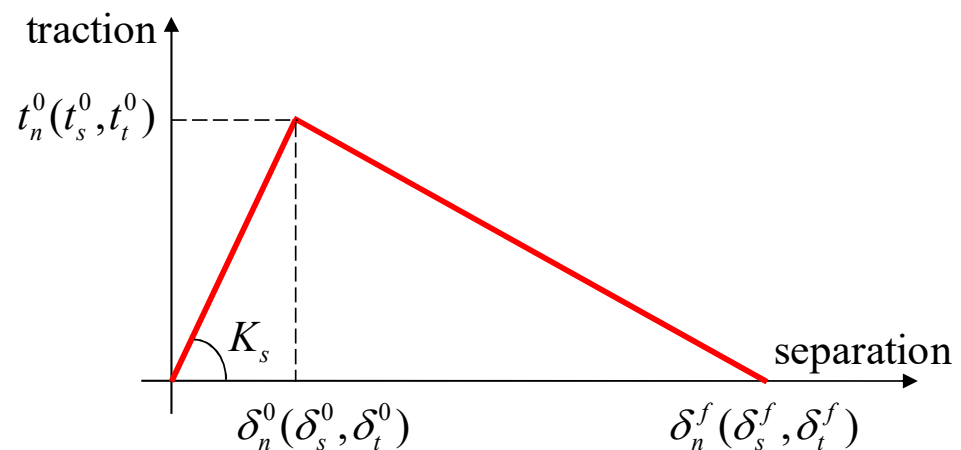


Figure 10. Typical traction-separation constitutive model.

The normal stiffness component, $K_n = 1358 \text{ N/mm}^3$, and the tangential stiffness components K_s and K_r are $20,358 \text{ N/mm}^3$.

The peak values of the traction stress components, the normal contact stress t_n and two shear contact stresses t_s and t_t , are 5.63 MPa .

The total plastic displacement is taken to be 0.241 mm .

5.3. Validation of FE Models

In analyzing the numerical results, we determined the first cracking loads at the interface or somewhere else in an FE model from the peak of the load versus principal stress curves, and the failure loads according to when the reinforcements yield or concrete fails on the compressive side. Table 6 compares the results obtained by FEA and tests for the seven groups of specimens. Most of the relative load differences listed in this table are less than 10% for the first crack loads and failure loads, which indicates that the FE models could predict the flexural behaviors that agree well with those test results. Furthermore, the locations of first cracks and failure that were predicted by the FE models coincide with those observed in the flexural tests for all the groups of specimens. These quantitative and qualitative comparisons could validate the constructed FE models for flexural behavior predictions of bridge deck panels with UHPFRC connections. However, it is also worth mentioning that the FE models would generally underestimate the failure loads. This might result from the fact that the adopted constitutive relationship, the elastic and perfectly plastic model of steel, deviates from the real stress versus strain curve when the reinforcement yields, since the reinforcing bars still could possess a slight strain hardening-like behavior in their yield stage.

Table 6. Comparisons of crack details and corresponding loads between FE models and tests.

FE Models	First Crack Load		Location of First Crack	Load of First Crack at Interface		Failure Load		Location of Failure
	FEA (kN)	Difference (%)		FEA/Test	FEA (kN)	Difference (%)	FEA (kN)	
M-N	21.8	8.4	NSC	N/A	N/A	104.9	10.8	NSC
M-U	44.6	6.7	UHPFRC	N/A	N/A	184.4	1.3	UHPFRC
J-R1	21.1	10.2	Interface	21.1	10.2	105.9	6.5	Interface
J-R2	22.5	10.4	NSC	30.8	9.9	116.5	5.7	NSC
J-R3	25.9	0.0	Interface	25.9	0.0	132.8	7.1	NSC
J-Z	25.2	−2.4	NSC	30.6 (A)/54.3 (B) ^a	2.9 (A)/9.2 (B) ^a	117.5	7.3	NSC
J-D	25.3	−4.5	NSC	40.3	7.9	109.8	5.7	NSC

Notes: (1)^a A and B herein represent the interfaces of A and B between NSC and UHPFRC for specimens of J-Z.

5.4. Parametric Analysis for UHPFRC-NSC Interface Treatment

5.4.1. Reinforcement Ratio and Mortise Hole Area Ratio

Discovered by the test results in the previous section, the higher reinforcement ratio within the UHPFRC joints and mortise holes at the interface could benefit the interfacial bonding performance. This subsection is meant to investigate how and how much these two factors influence the load (P_{cr}) corresponding to a first crack occurred at the interface by the validated FE models. To this end, we modified the FE models for J-R2 and J-R3 to respectively set different values of the mortise hole area ratio (R_h) and reinforcement ratio (R_f). The reinforcement ratio R_f in the UHPFRC connection was taken as 1.0%, 1.79%, 2.79%, 4.02%, 5.33%, 7.15%, and 9.05%. The mortise hole area ratio R_h was assigned a value of 0.0%, 0.52%, 2.09%, 3.27%, 4.71%, and 8.38%, respectively. Figure 11 illustrates the profiles of P_{cr} with changing ratios of R_f and R_h . As the two ratios of R_f and R_h grow, loads of P_{cr} get increased correspondingly. The curve with open circles indicates a critical minimal reinforcement ratio of 5.33%, which could be defined in such a manner that it ensures a load of first crack at an interface over 25.9 kN for a rectangular UHPFRC connection and thus leads to a first crack that would occur beyond the UHPFRC joint and its interface. It can also be confirmed by the test results of first-crack loads for specimens with rectangular UHPFRC connections and the monolithic specimen of M-N. In Figure 11, the other curve with solid circles roughly exhibits linearity, as the ratio of R_h is less than 3.27% that corresponds to the three mortise holes having a diameter of 25 mm. The further increase of R_h , however, does not achieve significant improvement in the load of P_{cr} . For a

compromise between the interfacial crack resistance and the reinforcement or mortise hole area ratio, it is recommended that the minimal ratios of R_f and R_h should be, respectively, 5.33% and 3.27%.

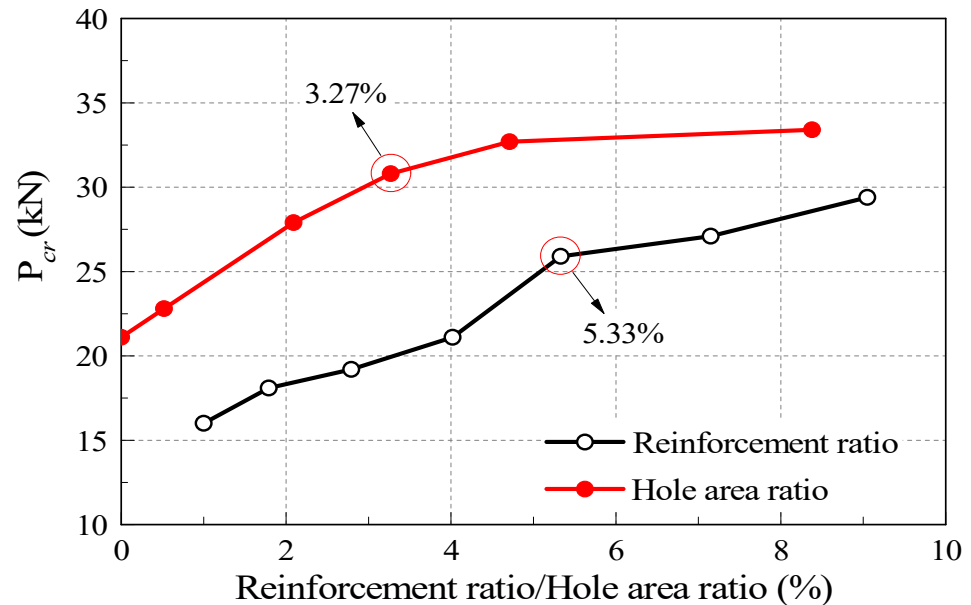


Figure 11. Load of first crack at interface versus reinforcement ratio and mortise hole area ratio.

5.4.2. Combined Interface Treatments

The aforementioned experimental and FEA results demonstrate convincingly that raising the reinforcement ratio, drilling mortise holes, or employing a Zigzag-shaped or diamond-shaped UHPFRC joint configuration is an effective means of enhancing the interfacial crack resistance considerably. In order to numerically ascertain how a combination of two of these ways can further improve the interfacial bonding performance, three types of FE models were developed to represent, respectively, a rectangular UHPFRC connection with an integration of denser reinforcement and mortise holes (labeled by J-R2+DR), and the Zigzag-shaped and diamond-shaped UHPFRC connections reinforced by compactly spaced reinforcing bars (labeled by J-Z+DR and J-D+DR). In these three FE models, the reinforcement and mortise hole area ratios took the suggested values, namely 5.33% and 3.27%. Since none of the final failures occurred at their interfaces for these FE models, we illustratively compared their loads P_{cr} with those obtained from FE models of J-R2, J-Z, and J-D in Figure 12. As expected, the use of combined interface treatments highly boosts the interfacial bonding performance. By comparison, the FE models with combined interface treatments achieved increased loads P_{cr} by 15.0% to 33.5%, in which the diamond-shaped UHPFRC connection configuration generated a superlative UHPFRC-NSC interface with the aid of a denser reinforcement.

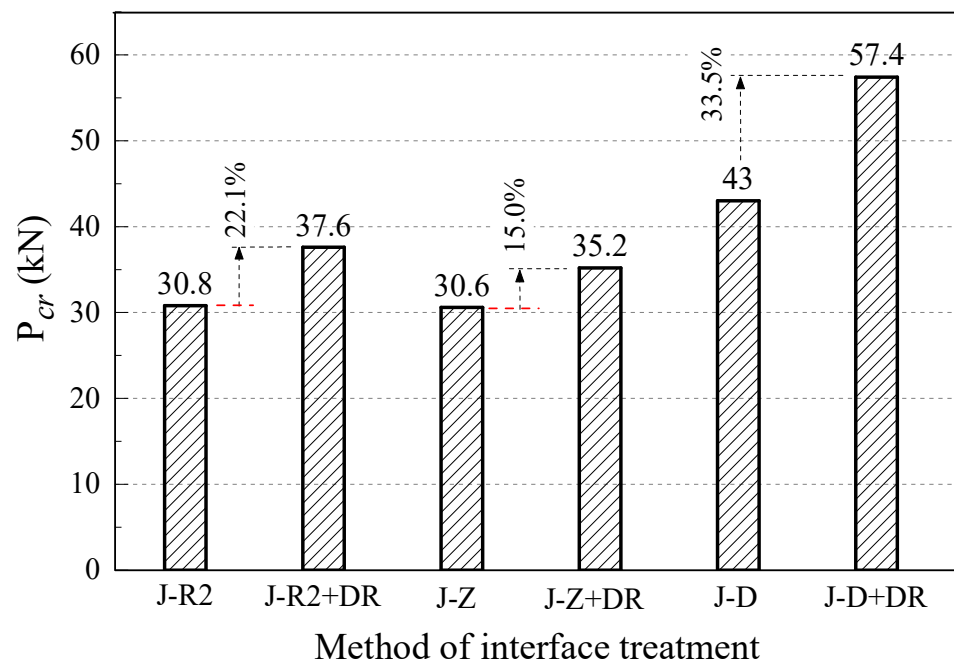


Figure 12. Comparisons of Loads (P_{cr}) of first crack at interfaces (DR represents denser reinforcement).

6. Conclusions

In the present study, we performed four-point bending tests to investigate the flexural behaviors of precast RC deck panels with different CIP UHPFRC connection configurations. The validated finite element models were then used to optimize the interface treatments. Based on the obtained results, the following conclusions have been drawn:

- (1) The CIP UHPFRC connection configurations and interface treatments under investigation could provide with adequate bonding strength at UHPFRC-NSC interfaces for precast RC deck panels.
- (2) The interfacial first-crack strengths of specimens J-R1 and J-R3 were basically comparable to that of the monolithic specimen M-N, whereas drilling mortise holes and applying Zigzag-shaped and diamond-shaped UHPFRC connections in J-R2, J-Z and J-D produced higher strengths by 43.7% to 96.2%. The specimens with UHPFRC connections exhibited failure loads comparable to or higher than M-N, and they did not fail at their interfaces with the exception of J-R1.
- (3) In comparison with the interfacial crack opening rates, drilling mortise holes at interfaces and increasing the reinforcement ratio within connections are considered as effective ways to enhance interface bonding performance, and so does applying a UHPFRC connection configuration as in J-D and J-Z.
- (4) The developed FE models are capable of predicting flexural behaviors of precast RC deck panels with UHPFRC connections. Numerical analyses suggest the critical minimal ratios of reinforcement and mortise holes to ensure sufficient interfacial crack resistance. The proposed combined interface treatments could highly increase the loads of first cracks at the interface.

Author Contributions: Conceptualization, Y.Z. and P.Z.; methodology, P.Z.; investigation, Z.Z.; writing—original draft preparation, Z.Z.; writing—review and editing, P.Z.; visualization, Z.Z.; supervision, Y.Z.; project administration, Y.Z.; funding acquisition, P.Z. All authors have read and agreed to the published version of the manuscript.

Funding: This research was funded by [the Natural Science Foundation of Hunan Province] grant number [2021JJ30131 and 2019JJ50120], [the Scientific research project of Education Department of Hunan Province] grant number [20C0611], and [the National Natural Science Foundation of China] grant number [51808212].

Institutional Review Board Statement: Not applicable.

Informed Consent Statement: Not applicable.

Data Availability Statement: The data used to support the findings of this study are available from the corresponding author upon request.

Conflicts of Interest: The authors declare no conflict of interest.

References

1. Kim, T.H.; Jin, B.; Kim, Y.J.; Kim, S.W.; Kim, I.H.; Shin, H.M. Inelastic Behavior of Precast Concrete Segmental Bridge Piers with Shear Resistance Connecting Structure. In Proceedings of the 14th World Conference on Earthquake Engineering, Beijing, China, 12–17 October 2008.
2. Momayez, A.; Ehsani, M.; Ramezani-pour, A.; Rajaie, H. Comparison of Methods for Evaluating Bond Strength between Concrete Substrate and Repair Materials. *Cem. Concr. Res.* **2005**, *35*, 748–757. [\[CrossRef\]](#)
3. Santos, D.S.; Santos, P.M.; da Costa, D.D. Effect of Surface Preparation and Bonding Agent on the Concrete-to-concrete Interface Strength. *Constr. Build. Mater.* **2012**, *37*, 102–110. [\[CrossRef\]](#)
4. He, W. The Research on the Interfacial Bond Strength of New-to-old Concrete. Master's Dissertation, Hunan University, Changsha, China, 2004. (In Chinese).
5. Santos, P.M.D.; Julio, E.N.B.S. Factors Affecting Bond between New and Old Concrete. *ACI Mater. J.* **2011**, *108*, 449–456. [\[CrossRef\]](#)
6. Wille, K.; Naaman, A.E.; El-Tawil, S.; Parra-Montesinos, G.J. Ultra-high Performance Concrete and Fiber Reinforced Concrete: Achieving Strength and Ductility without Heat Curing. *Mater. Struct.* **2012**, *45*, 309–324. [\[CrossRef\]](#)
7. Graybeal, B.A. *Material Property Characterization of Ultra-High Performance Concrete*; Tech. Rep. FHWA-HRT-06-103; Federal Highway Administration, U.S. Department of Transportation: Washington, DC, USA, 2006.
8. Graybeal, B.A. *Ultra-High Performance Concrete*; Tech. Rep. FHWA-HRT-11-038; Federal Highway Administration, U.S. Department of Transportation: Washington, DC, USA, 2011.
9. Pimienta, P.; Chanvillard, G. Durability of UHPFRC Specimens Kept in Various Aggressive Environments. In Proceedings of the 10th DBMC International Conference on Durability of Building Materials and Components, Lyon, France, 17–20 April 2005.
10. Haeri, H.; Sarfarazi, V.; Ebneabbasi, P.; Nazari Maram, A.; Shahbazian, A.; Marji, M.F.; Mohamadi, A.R. XFEM and experimental simulation of failure mechanism of non-persistent joints in mortar under compression. *Constr. Build. Mater.* **2020**, *236*, 117500. [\[CrossRef\]](#)
11. Haeri, H.; Mirshekari, N.; Sarfarazi, V.; Marji, M.F. Numerical simulation of compressive to tensile load conversion for determining the tensile strength of ultra-high performance concrete. *Smart Struct. Syst.* **2020**, *26*, 605–617.
12. Wang, X.W. Research on the Interfacial Shear Behavior of UHPC and Reinforced Concrete. Master's Thesis, Hunan University, Changsha, China, 2016. (In Chinese).
13. Tayeh, B.A.; Bakar, B.A.; Johari, M.M.; Voo, Y.L. Mechanical and Permeability Properties of the Interface between Normal Concrete Substrate and Ultra High Performance Fiber Concrete Overlay. *Constr. Build. Mater.* **2012**, *36*, 538–548. [\[CrossRef\]](#)
14. Tayeh, B.A.; Bakar, B.A.; Johari, M.M.; Voo, Y.L. Evaluation of Bond Strength between Normal Concrete Substrate and Ultra High Performance Fiber Concrete as a Repair Material. *Procedia Eng.* **2013**, *54*, 554–563. [\[CrossRef\]](#)
15. Carbonell Muñoz, M.A.; Harris, D.K.; Shann, S.V.; Ahlborn, T.M. Bond Strength between UHPC and Normal Strength Concrete (NSC) in accordance with Split Prism and Freeze-Thaw Cycling Tests. In *3rd International Symposium on UHPC and Nanotechnology for High Performance Construction Materials*; Kassel University Press: Kassel, Germany, 2012; pp. 377–384.
16. Carbonell Muñoz, M.A.; Harris, D.K.; Ahlborn, T.M.; Froster, D.C. Bond Performance between Ultrahigh-Performance Concrete and Normal-Strength Concrete. *J. Mater. Civ. Eng.* **2014**, *26*, 04014031. [\[CrossRef\]](#)
17. Hussein, H.H.; Sargand, S.M.; Rikabi, F.T.A.; Steinberg, E.P. Laboratory Evaluation of Ultrahigh-Performance Concrete Shear Key for Prestressed Adjacent Precast Concrete Box Girder Bridges. *J. Bridge Eng.* **2017**, *22*, 04016113. [\[CrossRef\]](#)
18. Graybeal, B.A. *Design and Construction of Field-cast UHPC Connections*; Tech. Rep. FHWA-HRT-14-084; Federal Highway Administration, U.S. Department of Transportation: Washington, DC, USA, 2014.
19. Graybeal, B.A. *Behavior of Field-Cast Ultra-High Performance Concrete Bridge Deck Connections under Cyclic and Static Structural Loading*; Tech. Rep. FHWA-HRT-11-023; Federal Highway Administration, U.S. Department of Transportation: Washington, DC, USA, 2010.
20. Arafa, A.; Farghaly, A.S.; Ahmed, E.A.; Benmokrane, B. Laboratory Testing of GFRP-RC Panels with UHPFRC Joints of the Nipigon River Cable-Stayed Bridge in Northwest Ontario, Canada. *J. Bridge Eng.* **2016**, *21*, 05016006. [\[CrossRef\]](#)
21. Russell, H.G.; Graybeal, B.A. *Ultra-High Performance Concrete: A State-of-the-Art Report for the Bridge Community*; Tech. Rep. FHWA-HRT-13-060; Federal Highway Administration, U.S. Department of Transportation: Washington, DC, USA, 2013.
22. *JGJ 55-2011*; Specification for Mix Proportion Design of Ordinary Concrete. Ministry of Housing and Urban-Rural Development: Beijing, China, 2011. (In Chinese)
23. *GB/T50081-2002*; Standard for Test Method of Mechanical Properties on Ordinary Concrete. Ministry of Housing and Urban-Rural Development: Beijing, China, 2003. (In Chinese)

24. GB/T 31387-2015; Reactive Powder Concrete. General Administration of Quality Supervision, Inspection and Quarantine: Beijing, China, 2015. (In Chinese)
25. GB50010-2010; Code for Design of Concrete Structures. Ministry of Housing and Urban-Rural Development: Beijing, China, 2010. (In Chinese)
26. Hussein, H.H.; Walsh, K.K.; Sargand, S.M.; Steinberg, E.P. Interfacial Properties of Ultrahigh-Performance Concrete and High-Strength Concrete Bridge Connections. *J. Mater. Civ. Eng.* **2016**, *28*, 04015208. [[CrossRef](#)]
27. JTG 3362-2018; Specifications for Design of Highway Reinforced Concrete and Prestressed Concrete Bridges and Culverts. Ministry of Transport of the People's Republic of China: Beijing, China, 2018. (In Chinese)
28. Chen, L.; Graybeal, B.A. *Finite Element Analysis of Ultra-High Performance Concrete: Modeling Structural Performance of an AASHTO Type II Girder and a 2nd Generation Pi-Girder*; Tech. Rep. FHWA-HRT-11-020; Federal Highway Administration, U.S. Department of Transportation: Washington, DC, USA, 2012.
29. Chen, L.; Graybeal, B.A. Modeling Structural Performance of Second-Generation Ultrahigh-Performance Concrete Pi-Girders. *J. Bridge Eng.* **2012**, *17*, 634–643. [[CrossRef](#)]
30. Kmiecik, P.; Kamiński, M. Modelling of Reinforced Concrete Structures and Composite Structures with Concrete Strength Degradation Taken into Consideration. *Arch. Civ. Mech. Eng.* **2011**, *11*, 623–636. [[CrossRef](#)]
31. Zhang, Z.; Shao, X.D.; Li, W.G.; Zhu, P.; Chen, H. Axial Tensile Behavior Test of Ultra High Performance Concrete. *China J. Highw. Transp.* **2015**, *28*, 50–58. (In Chinese)
32. Yang, J. Flexural Behavior of Ultra-high Performance Concrete Beams Prestressed with CFRP Tendons. Ph.D. Thesis, Hunan University, Changsha, China, 2007. (In Chinese).
33. Hussein, H.H.; Walsh, K.K.; Sargand, S.M.; Rikabi, F.T.A.; Steinberg, E.P. Modeling the Shear Connection in Adjacent Box-Beam Bridges with Ultrahigh-Performance Concrete Joints. I: Model Calibration and Validation. *J. Bridge Eng.* **2017**, *22*, 04017043. [[CrossRef](#)]
34. Dassault Systemes Simulia. *Analysis User's Manual*; ABAQUS Version 6.10; Dassault Systemes Simulia Corp.: Providence, RI, USA, 2011.